PAPER

Routes for nanoparticle translocation through polymer-brush-modified nanopores

IOP Publishing Journal of Physics: Condensed Matter
J. Phys.: Condens. Matter **30** (2018) 274006 (10pp) https://doi.org/10.1088/1361-648X/aac90b

Routes for nanoparticle translocation through polymer-brush-modified nanopores

Mario Tagliazucchi[1], **Kai Huang**[2] **and Igal Szleifer**[2]

[1] INQUIMAE-CONICET and DQIAQF-School of Sciences-University of Buenos Aires, Ciudad Universitaria, Pabellón 2, Ciudad Autónoma de Buenos Aires, C1428EHA, Argentina
[2] Department of Biomedical Engineering, Department of Chemistry and Chemistry of Life Processes Institute, Northwestern University, Evanston, IL 60208, United States of America

E-mail: igalsz@northwestern.edu

Received 14 March 2018, revised 23 May 2018
Accepted for publication 31 May 2018
Published 14 June 2018

Abstract

This work presents a theoretical study of the translocation routes of nanoparticles through polymer-brush modified nanopores. The calculations were performed with a molecular theory that explicitly accounts for the shape, size, conformations and interactions of all molecular species in the system. This work reports molecular-theory calculations allowing inhomogeneities in the three spatial dimensions, which allows us to study for the first time off-axis translocation routes, i.e. routes that do not coincide with the axis of the pore. Free-energy landscapes within the pore were obtained for particles of different sizes and affinity for the polymer brush. The minimum free-energy paths on these landscapes determine the translocation routes. Decreasing the size of the particle or increasing its affinity for the polymer, shifts the translocation route from the central axis of the pore towards its walls. Interestingly, for a given polymer-particle affinity, there exists an intermediate particle size that results in the most flat potential of mean force for translocation, therefore, that will optimize the rate of translocation.

Keywords: polymer-brush modified nanopores, translocation, potential of mean force

(Some figures may appear in colour only in the online journal)

1. Introduction

Mass transport under nanoconfinement is a process of fundamental relevance in life science and nanotechnology [1, 2]. Biology uses compartmentalization in living cells in order to spatially restrain chemical reactions and mass exchange. Biomolecules are exchanged between different compartments under the regulation of a variety of biological nanopores and channels such as the nuclear pore complex (NPC) and ion channels. These natural pores and channels have inspired research in synthetic nanopores [1, 3–7] with potential applications in biomedicine, environmental engineering and energy conversion. Polymer-coated solid-state nanopores have received special attention as the combination of soft and hard materials offers advantages in the function and intelligence of the artificial nanosystem. Here the intelligence or smartness of the nanopore refers to the ability of the system to respond to external stimuli such as temperature [8–10], pH [11, 12] or light [13, 14]. Stimuli-responsive polymers allow drastic on-demand changes in the presence of steric and electrostatic barriers for particle translocation, thus allowing for the fabrication of smart pores and channels with controllable transport properties. While swollen polymers naturally constitute a free energy barrier that blocks the passage of large inert objects through the nanopore, it is still unclear how different interactions between the particle and the polymer in a nanoconfined environment compete to determine the ability of the particle to translocate the pore. Such fundamental understanding is deeply needed to design nanopore devices.

The NPC is a paradigmatic example of selective biological transport, which remains unparalleled by man-made pores [15–19]. This pore is located in the nuclear membrane and it is responsible for the transport of almost all biomolecules between the cytoplasm and the nucleus. It is permeable to small molecules, such as water and ions, but bigger cargoes such as proteins and mRNA require the assistance of transport

receptors (known as karyopherins or 'kaps') to be effectively transported between the cytoplasm and the nucleus. The pore contains a series of disordered proteins (the FG-Nups, where 'FG' stands for phenylalanine-glycine, a recurring motif in the sequence of these proteins). Notably, the FG-Nups do not filter particles by their size: most proteins only enter the pore when bound to Kaps, but the kap-protein complexes are of course larger than the unbound proteins. Transport through the NPC is believed to be controlled by FG-Nup/kap interactions, both hydrophobic [20, 21] and electrostatic [19, 22]. Despite extensive study, the transport mechanism in the NPC remains elusive due to the challenge of analyzing the functional structure of the FG-Nups in nanoconfinement and the fact that the presence of cargo could in return reorganize the polymer inside the nanopore. In other words, the transport and the structure in polymer-functionalized nanopores could be strongly coupled. The general picture is clearly more complex than that described above, for example superresolution microcopy studies found that small molecules diffuse through the NPC via a central channel near pore axis, but large protein-cargoes follow a pathway close to the pore wall [23–25].

In this work, we address the thermodynamics of polymer translocation through polymer-modified nanopores with a molecular theory [19, 26–28]. The molecular theory explicitly considers the shape, size and conformation of the polymers and it has been proven to be a versatile tool for modeling polymer-grafted nanopores and obtaining thermodynamic information that is usually computationally challenging for molecular dynamics simulations. In our previous studies of particle translocation through polymer modified nanopores, we used the approximation of assuming a homogenous polymer distribution along the rotational direction of the cylindrical nanopore (i.e. we modeled an effectively two-dimensional axisymmetric problem) [19, 28]. This assumption restricted the position of the cargo to the axis of the pore because adding a nanoparticle off-axis would break the cylindrical symmetry of the system. In the present work, we present the first calculations allowing density inhomogeneities in the three spatial dimensions, which allows to fully map the free-energy landscape of the nanoparticle in all positions within the pore. We apply the theory to the case of a cylindrical pore modified by a neutral polymer brush and study the translocation of a spherical nanoparticle through the pore. We systematically studied the roles of particle size and the affinity of particle surface for the polymer segments on the free-energy landscape of the system. We found that for this relatively simple system, the nanoparticle would already experience a wealth of free-energy landscapes with distinctive topologies of the energy wells and barriers. In particular, we will show that the transport of the nanoparticle is path-selective based on the particle size and the polymer-particle interaction strength. We also determined the path of minimum free-energy for the particle translocation across the pore. This analysis show that, for a given particle size, there is an optimal polymer-particle interaction strength that minimizes the height of the free-energy barriers for translocation, and, therefore, should maximize the rate of translocation.

2. Theoretical methods

2.1. Formulation of the molecular theory

Our theoretical model is based on a previously developed molecular theory [19, 26–28]. We derive the theory starting from an approximate expression of the free energy of the system, which in the present case is a functional of the density of the solvent and the probability distribution of polymer conformations. The semigrand canonical free-energy functional for the system is

$$\beta F\left(\mathbf{R}\right) = \beta F_{\text{mixs}}\left(\mathbf{R}\right) + \beta F_{\text{conf}}\left(\mathbf{R}\right) + \beta F_{\text{ps}}\left(\mathbf{R}\right) \tag{1}$$

where $\mathbf{R}$ is the position of the particle, i.e. $\mathbf{R} = (R_x.\ R_y,\ R_z)$, and $\beta = 1/k_{\text{B}}\text{T}$ is the inverse temperature (k_{B} is Boltzmann's constant and T is temperature). The first term in equation (1) is the contribution to the free energy from the translational or mixing entropy of the solvent:

$$\beta F_{\text{mixs}}\left(\mathbf{R}\right) = \int \rho_{\text{s}}\left(\mathbf{r}\right)\left[\ln\left(\rho_{\text{s}}\left(\mathbf{r}\right)v_{\text{s}}\right) - 1\right]\mathrm{d}\mathbf{r} \tag{2}$$

where $\mathbf{r}$ is the position vector (i.e. $\mathbf{r} = (x, y, z)$). The integral in equation (2) runs over all the space that not occupied by the nanoparticle or the membrane, $\rho_{\text{s}}(\mathbf{r})$ is the number density of solvent molecules at position $\mathbf{r}$ and v_{s} is the molecular volume of the solvent.

The second term in equation (1) is the contribution from the conformational entropy of polymer chains,

$$\beta F_{\text{conf}}\left(\mathbf{R}\right) = \sum_{j}\sum_{\alpha} P\left(j,\alpha\right)\ln\left(P\left(j,\alpha\right)\right) \tag{3}$$

where $P(j, \alpha)$ is probability of finding the polymer chain j in the system in conformation α, the outer sum runs over all the polymer chains in the system and the inner sum over all the possible polymer conformations of these chains. The last term in F is the interaction energy between the nanoparticle and polymer segments,

$$\beta F_{\text{ps}}\left(\mathbf{R}\right) = \int \langle n_{\text{P}}\left(\mathbf{r}\right)\rangle \beta U_{\text{surf}}\left(\mathbf{r};\mathbf{R}\right)\mathrm{d}\mathbf{r}. \tag{4}$$

In this term, the integral runs over all the space that not occupied by the nanoparticle or the membrane and $\langle n_{\text{P}}(\mathbf{r})\rangle$ is the average number density of segments at $\mathbf{r}$, defined as:

$$\langle n_{\text{P}}(\mathbf{r})\rangle = \sum_{j}\sum_{\alpha} P\left(j,\alpha\right) n\left(\mathbf{r},j,\alpha\right) \tag{5}$$

where $n(\mathbf{r}, j, \alpha)\mathrm{d}\mathbf{r}$ is the number of segments that the chain j has in the volume element between $\mathbf{r}$ and $\mathbf{r} + \mathrm{d}\mathbf{r}$ when it is in conformation α. This function is given by the spatial distribution of segments of each conformation and it is an input to the theory. The function $U_{\text{surf}}(\mathbf{r}; \mathbf{R})$ is the particle-segment interaction energy between a segment at $\mathbf{r}$ and the particle at $\mathbf{R}$. We model this interaction with a square-well potential of the form:

$$U_{\text{surf}}(\mathbf{r};\mathbf{R}) = \begin{matrix} -\varepsilon_{\text{ps}} & R_{\text{p}} < |\mathbf{r}-\mathbf{R}| < \Delta + R_{\text{p}} \\ 0 & \text{otherwise} \end{matrix} \tag{6}$$

where ε_{ps} is the attraction energy of a segment within a distance Δ from the surface and R_{p} is the radius of the nanoparticle.

Repulsions are explicitly included in the model as excluded volume interactions for segment-nanoparticle, segment-wall and intramolecular segment–segment pairs. In other words, we consider only conformations that are self-avoiding and that do not overlap with the nanoparticle or pore walls. The remaining segment–segment, segment-solvent and solvent–solvent intermolecular repulsive interactions are considered through a packing constrain.

In order to find the equilibrium structure of the system, we determine the functional extremum of $F(\mathbf{R})$ with respect to $\rho_{\text{s}}(\mathbf{r})$ and $P(\alpha, j)$ subjected to two constrains. The first constraint is the packing constraint, which models intermolecular repulsive interactions:

$$\rho_{\text{s}}(\mathbf{r})\, v_{\text{s}} + \langle n_{\text{P}}(\mathbf{r})\rangle\, v_{\text{P}} = 1 \tag{7}$$

where v_{P} is the volume of a polymer segment. Note that equation (7) is defined only in the solution/polymer region (i.e. the region that is not part of the nanoparticle or the membrane). The second constraint is the normalization of the probability distribution function:

$$\sum_{\alpha} P(j,\alpha) = 1. \tag{8}$$

We consider these two constraints using the method of Lagrange multipliers. The functional to minimize therefore is:

$$W(\mathbf{R}) = F(\mathbf{R}) + \int \pi(\mathbf{r})\left[\rho_{\text{s}}(\mathbf{r})\, v_{\text{s}} + \langle n_{\text{P}}(\mathbf{r})\rangle\, v_{\text{P}} - 1\right] + \xi(j)\left[\sum_{\alpha} P(j,\alpha) - 1\right] \tag{9}$$

where $\pi(\mathbf{r})$ and $\xi(j)$ are the Lagrange multipliers associated to the packing constraint and the normalization of conformation probabilities, respectively. The equilibrium state of the system is given by the functional extrema of W with respect to $\rho_{\text{s}}(\mathbf{r})$ and $P(j,\alpha)$. The extremum with respect to $\rho_{\text{s}}(\mathbf{r})$ results in:

$$\rho_{\text{s}}(\mathbf{r})\, v_{\text{s}} = \exp\left[-v_{\text{s}}\beta\pi(\mathbf{r})\right]. \tag{10}$$

Note that $\pi(\mathbf{r})$, the Lagrange multiplier associate with the packing constraint, plays the role of a local osmotic pressure. Evaluating this expression in the bulk, allows to relate it to the known number density of solvent molecules in the bulk, $\rho_{\text{s}}^{\text{bulk}}$:

$$\begin{aligned}\rho_{\text{s}}(\mathbf{r}) &= \rho_{\text{s}}^{\text{bulk}} \exp\left[-v_{\text{w}}\beta\left(\pi(\mathbf{r}) - \pi^{\text{bulk}}\right)\right] \\ &= \rho_{\text{s}}^{\text{bulk}} \exp\left[-v_{\text{w}}\beta\pi'(\mathbf{r})\right]\end{aligned} \tag{11}$$

where $\pi'(\mathbf{r}) = \pi(\mathbf{r}) - \pi^{\text{bulk}}$. The minimization of W with respect to $P(\alpha, j)$ yields

$$P(j,\alpha) = \frac{1}{q(j)} \exp\left[-\int n(\mathbf{r},\alpha,j)\, v_{\text{P}}\beta\pi(\mathbf{r})\, \mathrm{d}\mathbf{r} - \int n(\mathbf{r},\alpha,j)\,\beta U_{\text{surf}}(\mathbf{r},\mathbf{R}_{\text{p}})\mathrm{d}\mathbf{r}\right] \tag{12}$$

where $q(j)$ is a single-chain partition function, which is related to the Lagrange multiplier $\xi(j)$ that enforced the normalization of the probabilities by $q(j) = 1/\exp(1+\xi(j))$. We can rewrite equation (12) in order to introduce $\pi'(\mathbf{r})$ as:

$$P(j,\alpha) = \frac{1}{q'(j)} \exp\left[-\int n(\mathbf{r},\alpha,j)\, v_{\text{P}}\beta\pi'(\mathbf{r})\, \mathrm{d}\mathbf{r} - \int n(\mathbf{r},\alpha,j)\,\beta U_{\text{surf}}(\mathbf{r},\mathbf{R})\mathrm{d}\mathbf{r}\right] \tag{13}$$

where $q'(j) = q(j)\exp\left(v_{\text{P}}\beta\pi^{\text{bulk}}N\right)$ and N is the chain length (segments per polymer).

2.2. Numerical discretization and solving

In order to solve the theory, equations (11) and (13) are inserted into the packing constraint, equation (7) and the resulting equation is discretized in the x, y and z coordinates using a discretization step of $\Delta = 0.5$ nm. Note that the value of $q'(j)$ results from replacing equation (13) into the probability normalization constraint, equation (8).

The description of the curved surfaces of the nanoparticle and the pore using a cubic lattice necessarily involves lattice sites that are part particle or part membrane and part solution. In order to deal with these sites, we consider the available volume that is accessible for the solution in each of them. Let us first rewrite the equations of the theory introducing the mask function $h(\mathbf{r})$, so that $h(\mathbf{r}) = 0$ if the point $\mathbf{r}$ is part of the membrane or the particle and $h(\mathbf{r}) = 1$ if the point $\mathbf{r}$ is part of the solution. For example, equation (1) becomes:

$$\begin{aligned}\beta F(\mathbf{R}) = &\int \rho_{\text{s}}(\mathbf{r})\left[\ln\left(\rho_{\text{s}}(\mathbf{r})\, v_{\text{s}}\right) - 1\right] h(\mathbf{r})\, \mathrm{d}\mathbf{r} \\ &+ \sum_{j}\sum_{\alpha} P(j,\alpha)\ln\left(P(j,\alpha)\right) \\ &+ \int \langle n_{\text{P}}(\mathbf{r})\rangle\beta U_{\text{surf}}(\mathbf{r};\mathbf{R})\, h(\mathbf{r})\, \mathrm{d}\mathbf{r}\end{aligned} \tag{14}$$

where the integrals now run over the entire space. Equation (13) becomes:

$$P(j,\alpha) = \frac{1}{q'(j)} \exp\left[-\int n(\mathbf{r},\alpha,j)\, v_{\text{P}}\beta\pi'(\mathbf{r})\, h(\mathbf{r})\, \mathrm{d}\mathbf{r} - \int n(\mathbf{r},\alpha,j)\,\beta U_{\text{surf}}(\mathbf{r},\mathbf{R})h(\mathbf{r})\,\mathrm{d}\mathbf{r}\right]. \tag{15}$$

We then discretize the resulting equations by transforming integrals over $\mathbf{r} = (x, y, z)$ into sums over the cells of the lattice. While in the computational implementation of the theory it is useful to use three variables to index the x, y and z coordinates of each cell, let us use here a single variable to simplify the notation, i.e. each cell has an index i, with $i = 1$ to M. In the discretization procedure, we replace $h(\mathbf{r})$ by its discretized version, $\bar{h}(i)$, which is the volume fraction of the cell i that it is occupied by either solvent or polymer segments. We compute $\bar{h}(i)$ as:

$$\bar{h}(i) = \frac{1}{\Delta^3}\int_{\text{cell } i} h(\mathbf{r})\mathrm{d}\mathbf{r} \tag{16}$$

where the integration is performed over cell i.

The discretized version of equation (1) is:

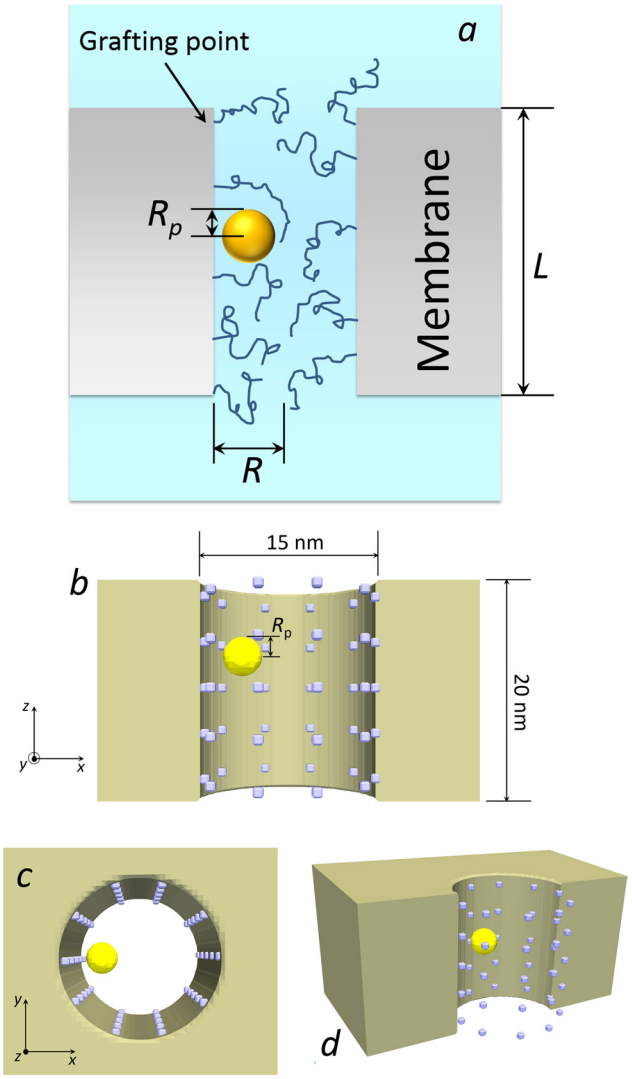

Figure 1. (a) Cartoon of the polymer-modified pore studied in this work. (b)–(d) Side (b), top (c) and perspective (d) cuts of the polymer-modified nanopore. The nanoparticle is shown in yellow. The blue dots in panels (b), (c) and (d) indicate the position of the grafting points of the polymer chains on the inner pore surfaces.

$$\beta F(\mathbf{R}) = \sum_{i=1}^{M} \rho_s(i)\left[\ln(\rho_s(i)\nu_s) - 1\right]\bar{h}(i)\Delta^3 + \sum_j \sum_\alpha P(j,\alpha)\ln(P(j,\alpha)) + \sum_{i=1}^{M} \langle n_P(i)\rangle \beta \bar{U}_{surf}(i;\mathbf{R})\bar{h}(i)\Delta^3 \quad (17)$$

where $\bar{U}_{surf}(i;\mathbf{R})$ is calculated as:

$$\bar{U}_{surf}(i;\mathbf{R}) = \frac{1}{\Delta^3}\int_{cell\ i} U_{surf}(\mathbf{r};\mathbf{R})h(\mathbf{r})\,d\mathbf{r}. \quad (18)$$

The discretized form of equation (13) is:

$$P(j,\alpha) = \frac{1}{q'(j)}\exp\left[-\sum_{i=1}^{M}\nu_P\beta\pi'(i)n(i,\alpha,j) - \sum_{i=1}^{M}\beta\bar{U}_{surf}(i,\mathbf{R})n(i,j,\alpha)\right] \quad (19)$$

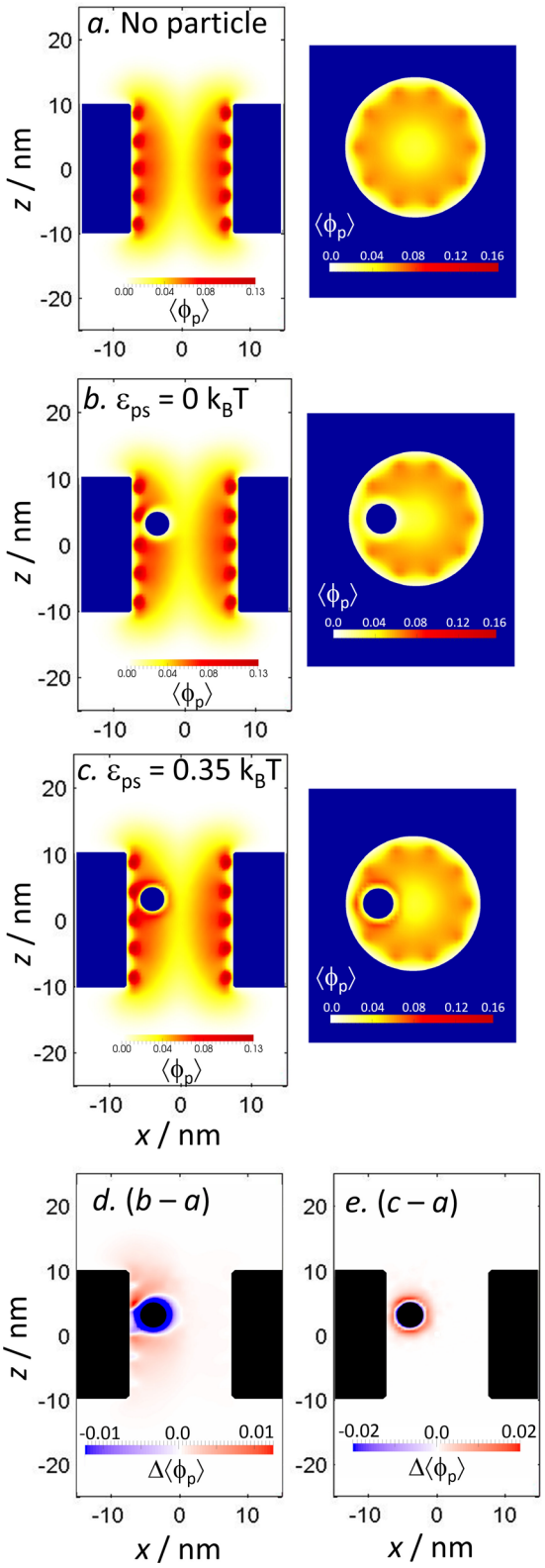

Figure 2. (a)–(c) Color maps of the volume fraction of the polymer on the x–z plane containing the pore axis (left panels) and a x–y plane perpendicular to the pore axis (right panels). The plots correspond to systems without nanoparticles (panel (a)) or nanoparticles of radius $R_p = 2$ nm, located at $R_x = -4$ nm, $R_y = 0$ nm and $R_z = 3$ nm with polymer-nanoparticle interaction strengths of $\varepsilon_{ps} = 0$ k_BT (panel (b)) or 0.35 k_BT (panel (c)). (d) and (e). Color maps showing the difference between the volume fractions of the polymer between panels (b) and (a) (panel (d)) and between panels (c) and (a) (panel (e)).

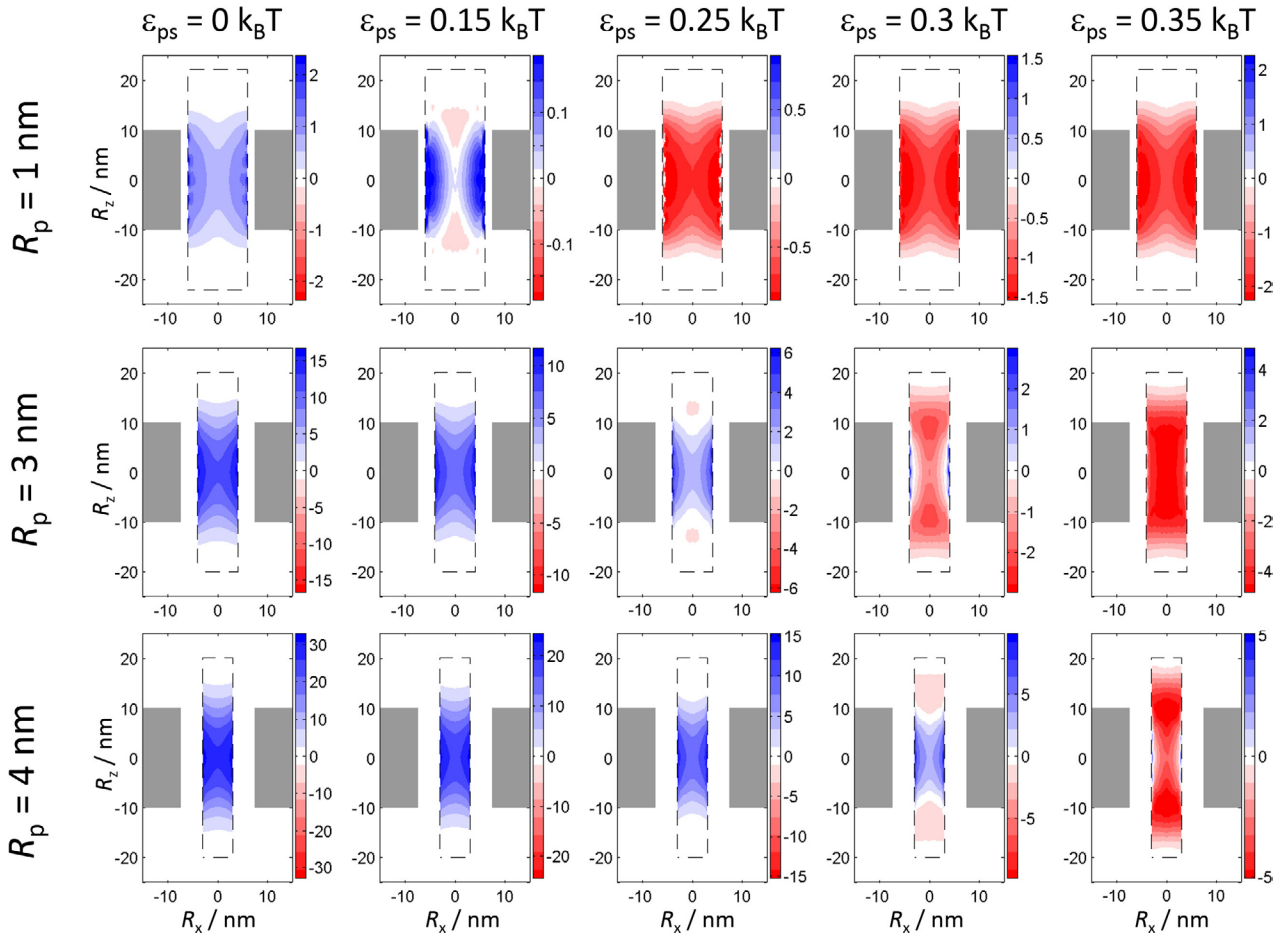

Figure 3. Color maps of the free energy of nanoparticle-pore systems (in units of k_BT) as a function of R_x and R_z (x and z coordinates of the center of the nanoparticle). In all cases, $R_y = 0$. Results are shown for different particle radius (R_p) and particle-segment attraction strengths (ε_{ps}). The rectangle with dashed lines indicates the region of the pore where the calculations have been performed. Note that the minimum distance between the center of the particle and the surface of the pore is R_p, thus the size of the rectangle in R_x decreases as R_p increases.

where $n(j,\alpha,i)$ is the number of segments that the chain j in conformation α has in the cell i. Note that, according to this definition, equation (5) is discretized as:

$$\langle n_P(i)\rangle = \frac{1}{\Delta^3 \bar{h}\,(i)} \sum_j \sum_\alpha P\,(j,\alpha)\, n\,(i,j,\alpha). \qquad (20)$$

2.3. Molecular model

Our theoretical methodology requires a set of all the possible conformations of the polymer chains, which enters into the theory through the spatial distribution of segments in each conformation, i.e. the function $n(\mathbf{r},j,\alpha)$. While the theory considers in principle all possible conformations, it is enough to use a very large set of conformations instead. We found that using 10^6 conformations is enough to produce converged statistics for the conditions investigated in this work. These conformations are generated using the rotational isomeric (RIS) model [29] with a segment length of 0.5 nm. The volumes of solvent molecules and segments were 0.03 and 0.113 nm^3, respectively. The thickness of the potential well in equation (6) was taken as 0.5 nm.

2.4. Calculation of the minimum free energy paths (MFEP)

In order to calculate the MFEP for particle translocation, we determine first the free energy of the particle as a function of its position, i.e. we calculate $F(\mathbf{R})$ as a function of $\mathbf{R}$. We then determine the MFEP over the resulting surface using the improved string method of Weinan *et al* [30]. We fix the two ends of the string (i.e. initial and final particle positions) on the pore central axis ($x = y = 0$) and $z = \pm$ 16 nm. We sampled the MFEP with a string of 20 beads.

3. Results

Figure 1 depicts the system under study. We consider a short cylindrical nanopore of radius $R = 7.5$ nm and length $L = 20$ nm connecting two identical reservoirs. The origin of coordinates is set to the geometrical center of the pore. The inner walls of the pore are coated by polymer brushes. In the case of the pore in figure 1, there are 50 polymer chains, distributed in five rings with ten polymers per ring, which yields a surface coverage of 0.053 chains · nm^{-2} (we will also consider below an example with a larger grafting density). The

chain length is fixed to $N = 40$. The spherical nanoparticle of radius R_p is located at position $\mathbf{R} = (R_x, R_y, R_z)$.

Figure 2(a) shows the density of the polymer in the absence of a nanoparticle inside the pore. The density of the polymer is larger near the walls than in the central axis of the channel and there is some density at the entrances of the pore. This density is due to chains that stretch towards the reservoirs in order avoid unfavorable polymer-polymer repulsions [26, 31]. In figure 2(b), we show the density of the polymer in the presence of a nanoparticle with a neutral surface (i.e. a surface that does not attract the polymer segments, $\varepsilon_{ps} = 0$ k_BT). There is a depletion in the polymer density around the particle, up to a distance of ~ 1 nm from the particle surface (see the blue region in figure 2(d), which shows the difference between the polymer density in the presence and absence of the particle). The depletion of polymer near the particle has an entropic origin: the presence of the particle decreases the number of polymer conformations that can explore the region close to the particle (this effect is similar to that observed for the polymer density of brushes near the neutral grafting surface [32, 33]). The polymer that is expelled from the position of the particle and its surroundings is redistributed in a large region of the pore (red region in figure 2(d)). In the case where there are attractive particle-segment interactions (figure 2(c), $\varepsilon_{ps} = 0.35$ k_BT), there is an increase in the density of the polymer surrounding the particle. Note that in this case, the change in polymer density away from the particle is much smaller than that near the particle and thus it cannot be observed in the color scale of the difference plot in figure 2(e).

Let us now focus on the free-energy landscape that results from placing the particle in different positions within the pore. Since we will report free-energy differences, we find it convenient to set the zero for the particle in the bulk (i.e. far away from the pore). We will scan the position of the particle in the x and z coordinates (R_x and R_z) and fix $R_y = 0$. In a pore with a perfect cylindrical symmetry, scanning only R_x and R_z is enough to completely map the free-energy landscape. In the present case, however, the cylindrical symmetry of the pore is slightly perturbed by the presence of the grafting points. Thus our mapping procedure is not exhaustive, although it is enough to provide a general picture of the free-energy surface.

Figure 3 shows color maps of the free-energy differences as a function of the position of the particle in the pore for different particle sizes and particle-segment attraction strengths (ε_{ps}). The blue regions indicate positions where the particle has a free-energy larger than in the bulk, thus the particle will be repelled from these regions. The red regions indicate a free-energy smaller than in the bulk, thus these regions attract the particle. For $\varepsilon_{ps} = 0$, the particle-pore interaction is always repulsive and the magnitude of the repulsion increases with increasing local polymer concentration. The origin of the repulsive interaction is the loss of polymer and solvent entropy that occurs when the particle is inserted into the pore. The entropy of the polymer decreases upon particle insertion because there is a decrease in the number of allowed conformations. The decrease in solvent entropy is originated from the fact that the polymer segments in the region where

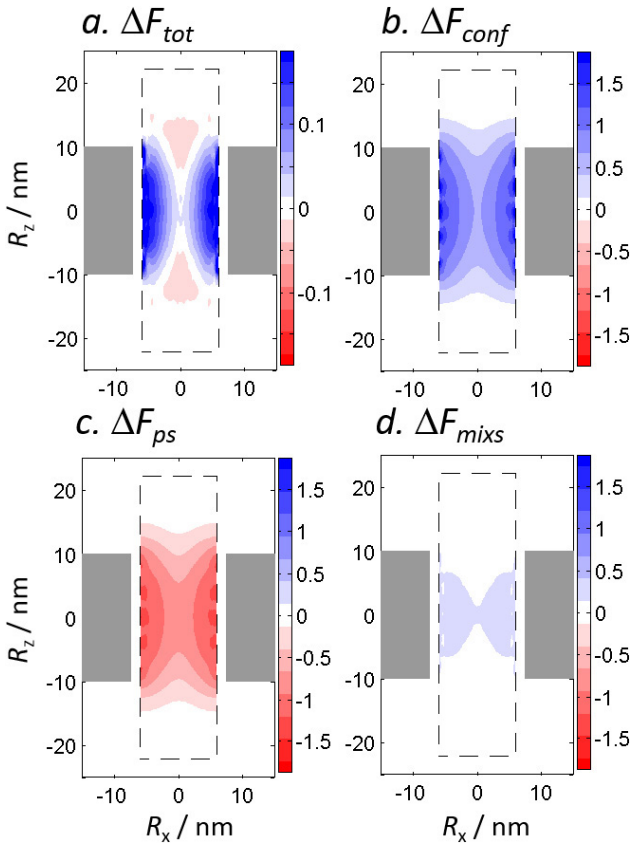

Figure 4. Color maps of the free energy contributions of a nanoparticle-pore system (in units of k_BT) as a function of R_x and R_z ($R_y = 0$). Results correspond to $R_p = 1$ nm and $\varepsilon_{ps} = 0.15$ k_BT. The panels show the total free energy (panel (a)) and the contribution to the free energy arising from: conformational entropy of the polymer chains (panel (b)), the particle-segment attractions (panel (c)) and the mixing entropy of the solvent (panel (d)).

the particle is inserted must be redistributed to other regions of the pore, thus increasing the average polymer density (this effect is clearly observed as a red region spanning a large part of the pore in the difference plot of figure 2(d)). As the density of the polymer inside pore increases, the solvent must flow from the pore (where its concentration is small) to the bulk (where its concentration is large), which decreases its mixing entropy.

As the particle-segment attraction strength increases (increasing ε_{ps}), figure 3 shows a transition from a repulsive potential to an attractive potential. On the other hand, increasing the radius of the particle (for a fixed ε_{ps}) results in a transition from attractive to repulsive potentials. The reason for this effect is that the strength of the entropic repulsion scales with particle volume ($\sim R_p^3$), while the particle-segment attraction scales with particle area ($\sim R_p^2$). Therefore, increasing the size of the particle increases repulsive interactions more than it increases particle-segment attractions.

For the largest attraction strength under study ($\varepsilon_{ps} = 0.35$ k_BT) and small particles ($R_p = 1$ nm), figure 3 shows that the pore-particle attraction is strongest near pore walls, but for large particles ($R_p = 4$ nm) the attraction is strongest near the pore axis. We will come back to this point at the end of this work when discussing the pathways of translocation.

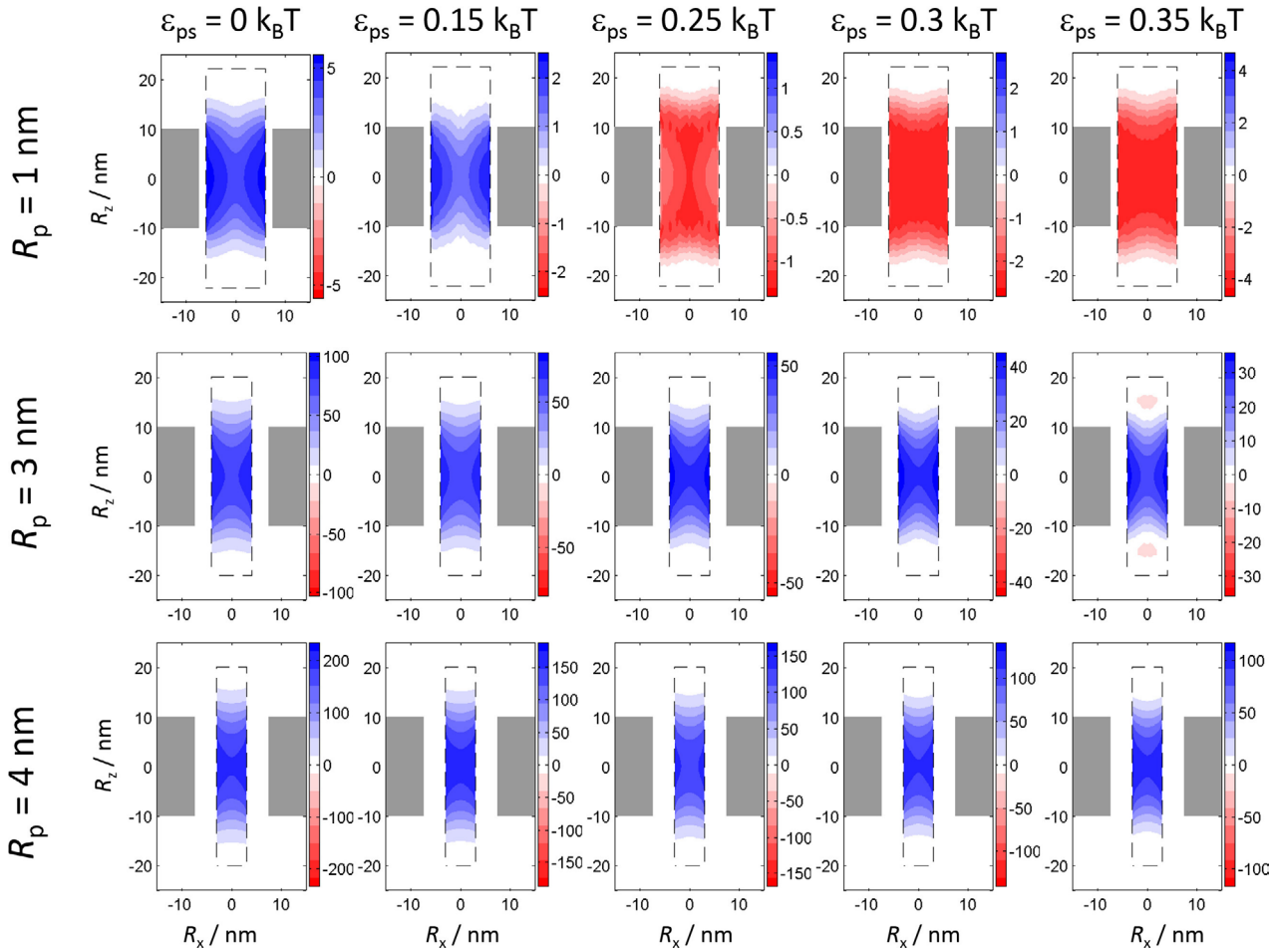

Figure 5. Same as figure 3 but for a pore containing 200 chains instead of 50 chains. The chains are arranged in ten rings with 20 polymers per ring, which yields a surface coverage of 0.21 chains · nm^{-2}.

As the particle-segment attraction strength increases, figure 3 shows that the potential turns attractive first at the entrances of the pore (see for example the plot for $\varepsilon_{ps} = 0.15$ k_BT and $R_p = 1$ nm). In figure 4, we analyze this effect in detail by plotting the three contributions to the free energy (see equation (1)): the contribution from the conformational entropy of the polymer (ΔF_{conf}), the contribution from the mixing entropy of the solvent (ΔF_{mixs}) and the particle-segment attraction energy (ΔF_{ps}). The plot shows that the total free energy depends mainly on the competition between ΔF_{conf} and ΔF_{ps}. These two quantities scale differently with the local density of the polymer, which causes that, upon increasing ε_{ps}, the region near the entrance of the pore (low local polymer density) turns attractive before the region near the walls of the pore (high local polymer density). The presence of free-energy wells at each entrance of the nanopore is interesting as these wells may serve to trap and concentrate the particles prior translocation. While for the specific case of the results in figure 4, the depth of the wells (~0.025 k_BT, see the scale of the color map in figure 4(a)) is not deep enough to trap a particle, we have observed deeper wells for larger particles (i.e. see plot for $R_p = 4$ nm, $\varepsilon_{ps} = 0.3$ k_BT in figure 3).

In figure 5, we explore the effect of increasing the surface coverage of the polymer by a factor of four. The general trends described above for the low-surface coverage case in figure 3 are still observed. Comparison of figures 3 and 5, shows that increasing the surface coverage (for fixed R_p and ε_{ps}) makes the particle-pore interaction more repulsive. This result is explained by the fact that the repulsive (ΔF_{conf} and ΔF_{mixs}) and the attractive (ΔF_{ps}) contributions to the free energy scale differently with polymer density. More precisely, the results in figures 4 and 5 indicate that upon increasing polymer density, the repulsive contributions to the free energy increase faster than the attractive ones.

We will now analyze the routes for nanoparticle translocation (all calculations correspond to the low-surface-density case). Assuming that the timescale of particle motion is much slower than that of polymer reorganization, we can decouple the motion of the particle from that of the polymers and determine the minimum free-energy path (MFEP) for the translocation of the particle through the channel using the free-energy landscapes determined above. We found these curves on the different potentials using the improved string method [30], fixing the origin and end points at the entrances of the pore. The improved string employs a string of beads connecting the two points and describing a curve on the free-energy surface. Initially, the beads do not necessarily sit on the minimum free-energy path. Each of the beads is then moved against the

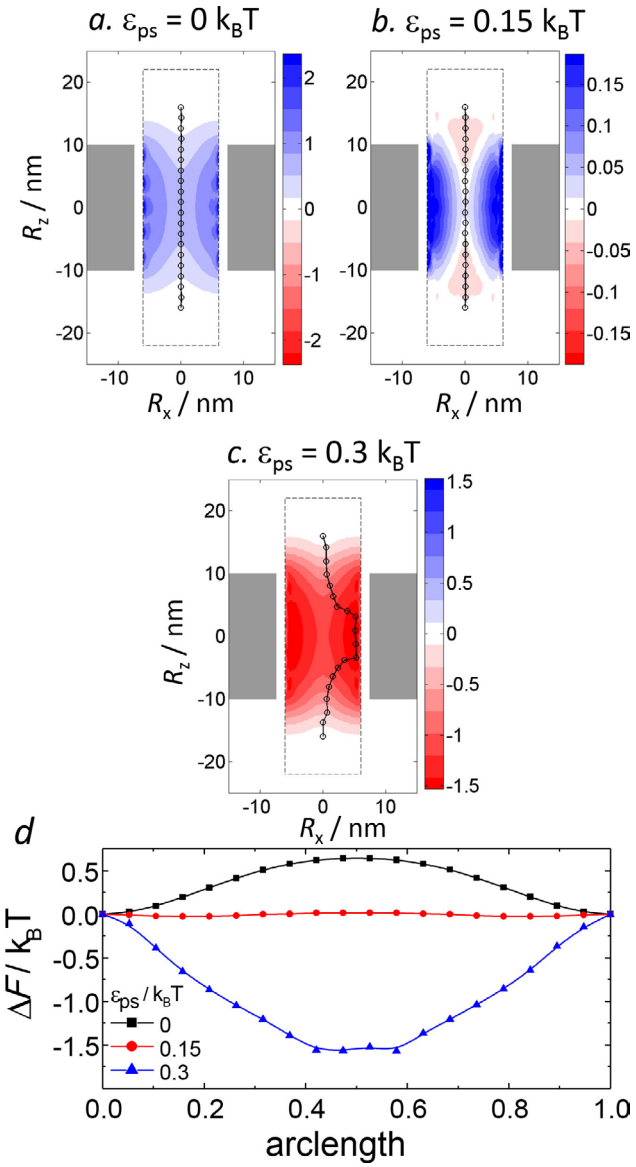

Figure 6. (a)–(c) Color maps of the free energy contributions of a nanoparticle-pore system (in units of k_BT) as a function of R_x and R_z ($R_y = 0$). Results correspond to $R_p = 1$ nm and different values of ε_{ps}. The black line with circles in each plot shows the minimum free-energy path for the translocation of the particle through the pore. Panel (d) shows the respective values of the free energies along the minimum free-energy paths.

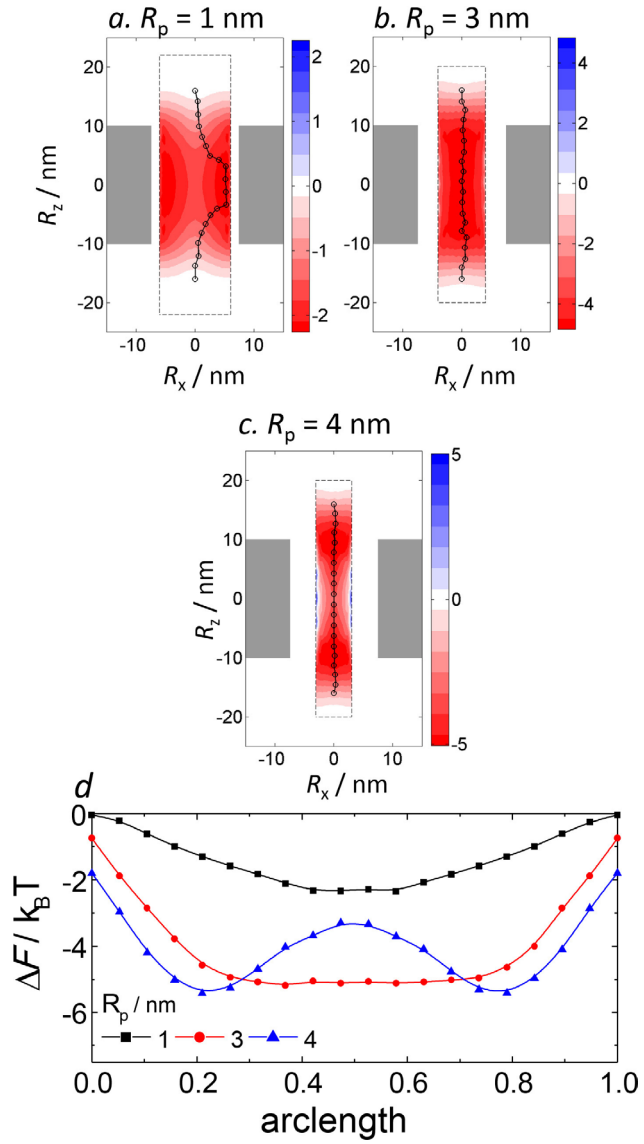

Figure 7. Same as figure 6 but for $\varepsilon_{ps} = 0.35$ k_BT and different values of the particle radius, R_p.

direction of the local free-energy gradient (i.e. it is moved downhill free energy), while enforcing that the arclength distances between neighbor beads are equal for each pair of neighbors. In practice, the method successively alternates downhill free-energy moves with string reparametrization steps. Upon convergence of the method (when the string does not change anymore with successive move/reparametrization steps) the resulting string describes the minimum free-energy path between its two extremes.

Figure 6 shows the effect of the attraction strength, ε_{ps}, on the MFEP. For a neutral particle surface (figure 6(a), $\varepsilon_{ps} = 0$) the potential is repulsive and the MFEP coincides with the pore axis. When the potential becomes attractive (figure 6(c), $\varepsilon_{ps} = 0.3$ k_BT), the MFEP gets close to the wall of the pore. Figure 6(d) shows the free energy as a function of the position along the MFEP (i.e. the arclength of the curve). For $\varepsilon_{ps} = 0$ (example in figure 6(a)), the plot shows a free-energy barrier. If the height of the free-energy barrier is smaller than or similar to the thermal energy (k_BT), translocation of the particle is expected. In the case of $\varepsilon_{ps} = 0.3$ k_BT (example in figure 6(c)), the free-energy profile experiences a well, where the particle can get trapped. Therefore, in order to translocate through the pore, the particle should overcome a barrier equal to the depth of this well. Interestingly, for the case of $\varepsilon_{ps} = 0.15$ k_BT (example in figure 6(b)), the profile is almost flat, showing only two very shallow wells at the entrances of the pore separated by a low barrier of 0.04 k_BT (note that the scales of the color maps in figures 6(a)–(c) are different). It is known that diffusion on a 1D potential is fastest when the potential is flat [34]. A similar proof for diffusion on 2D is not available, although numerical and analytical results suggests a similar situation [35, 36]. Therefore, one expects that translocation of the particle through the pore will be fastest

for the value of ε_{ps} that results in the flattest potential (i.e. the potential that has the minimum free-energy difference between wells and barriers). Hence, our results suggest that it is possible to optimize the rate of particle translocation by carefully modulating the particle-segment attraction.

In figure 7, we consider the case of a strongly attractive particle-polymer interaction ($\varepsilon_{ps} = 0.35$ k_BT) for particles of different size. We observe that the MFEP overlaps the pore axis for large particles ($R_p = 3$ and 4 nm, figure 7(c)) and shifts to the walls for small particles ($R_p = 1$ nm). In other words, in the case of strongly attractive particle-polymer interactions, two different translocation routes are possible: translocation through the axis for large particle vs. translocation near the walls for small particles.

4. Conclusions

In summary, we have studied for the first time the free-energy landscape for the translocation of a particle through a polymer-modified nanopore allowing off-axis particle positions. These calculations are possible because we performed fully 3D molecular-theory calculations. These calculations are a significant improvement to our previous work [19, 28], which used 2D calculations with cylindrical symmetry, thus restricting the particle positions to reside on pore axis. We systematically explored the effects of particle size, particle-segment attraction strength and polymer surface coverage on the free-energy landscape.

In order to study the translocation route of the nanoparticle, we determined the MFEP for the translocation of the particles on this landscape. The MFEP determined in this work uses our free-energy calculations for fixed particle positions, and thus they correspond in essence to a potential of mean-force. In other words, our MFEP are the routes that the particle will follow if polymer equilibration occurs much faster than nanoparticle motion, which should be a good approximation for large particles. In principle, a less constrained determination of the MFEP is possible, where the degrees of freedom of the polymer and the position of the particle are treated at the same level [37]. Such calculation is feasible using the recently derived MFEP/Molecular Theory methodology [38], but it will be highly demanding in terms of computational resources. Moreover, based on literature results [37], we expect that the free-energy barriers and wells for the fully unconstrained calculation will be similar to those reported here.

An interesting finding is that by carefully balancing the particle-segment interaction and the particle size it is possible to achieve an almost flat MFEP. This result implies that for a family of particles with similar surface chemistry (ε_{ps}) but different radii (R_p), there will be an optimal radius that will yield the flattest possible potential (larger and smaller particles will experience more repulsive or attractive potentials, respectively). This finding can have implications for transport through the NPC, where large cargoes can transverse the NPC faster than smaller ones, providing that the cargo-pore interaction is adequate (which in the case of the NPC is regulated by the formation of complexes with Kaps).

The size of the particle and segment-particle interaction have important consequences for the translocation route. For a particle of fixed size, increasing the particle-segment interaction shifts the translocation pathway from the axis of the channel toward its walls. Under a constant particle-segment attraction strength, smaller particles take a translocation path closer to the wall than that of the larger ones. A path-selective transport mechanism could reduce the competition between different cargoes and make the overall cargo traffic more organized and efficient. This strategy is especially useful in the NPC, where many different cargoes of varying sizes and binding strengths to the FG-Nups have to be exchanged between the two sides of the nanopore. Interestingly, recent superresolution microscopy experiments of the NPC [23, 24] have revealed the presence of different translocation pathways. One of these experiments [24] have shown that molecules without bound Kaps diffused along the axis of the pore (for Mw < 70 kDa). On the other hand, free Kaps (Mw $= 102$ kDa) followed a peripheral route, which suggests that the attractive Kap/FG-Nup interactions dominate over the increase in the molecular weight and thus the transport route shifts from the axis towards the walls. Interestingly, Kap-cargo complexes (Mw $= 217$ kDa) displayed a peripheral translocation route, but that it is closer to the axis of the pore than that of the Kap alone, which suggests that in these two cases the Kap/FG-Nup attractions are similar and the translocation route is mainly determined size.

Future work will extend our study to consider the effect of electrostatic interactions on the free-energy landscape of cargo translocating across a polyelectrolyte-coated nanopore, since charge effects has been revealed to be important in our previous model of the NPC [19]. The insights from our systematical 3D modeling presented here constitute a first step for the understanding complex transport behaviors under nanoconfinement and the rational design of smart artificial nanopores.

Acknowledgment

KH and IS acknowledge financial support from the National Science Foundation Grant CBET-1403058. MT is a fellow of CONICET and acknowledges financial support from Agencia Nacional de Promoción Científica y Tecnológica (ANPCyT) (PICT-0099-2015, PICT 0154-2016).

ORCID iDs

Mario Tagliazucchi https://orcid.org/0000-0003-4755-955X
Kai Huang https://orcid.org/0000-0001-8400-9341
Igal Szleifer https://orcid.org/0000-0002-8708-0335

References

[1] Tagliazucchi M and Szleifer I 2015 Transport mechanisms in nanopores and nanochannels: can we mimic nature? *Mater. Today* **18** 131–42
[2] Tagliazucchi M and Szleifer I 2016 *Chemically Modified Nanopores and Nanochannels* (New York: Elsevier)

[3] Wen L P, Hou X, Tian Y, Nie F Q, Song Y L, Zhai J and Jiang L 2010 Bioinspired smart gating of nanochannels toward photoelectric-conversion systems *Adv. Mater.* **22** 1021–4

[4] Zhang Z, Wen L and Jiang L 2018 Bioinspired smart asymmetric nanochannel membranes *Chem. Soc. Rev.* **47** 322–56

[5] Hou X, Guo W and Jiang L 2011 Biomimetic smart nanopores and nanochannels *Chem. Soc. Rev.* **40** 2385–401

[6] Brunsen A, Díaz C, Pietrasanta L I, Yameen B, Ceolín M, Soler-Illia G J A A and Azzaroni O 2012 Proton and calcium-gated ionic mesochannels: phosphate-bearing polymer brushes hosted in mesoporous thin films as biomimetic interfacial architectures *Langmuir* **28** 3583–92

[7] Kowalczyk S W, Blosser T R and Dekker C 2011 Biomimetic nanopores: learning from and about nature *Trends Biotechnol.* **29** 607–14

[8] Guo W *et al* 2010 Current rectification in temperature-responsive single nanopores *ChemPhysChem* **11** 859–64

[9] Zhou Y, Guo W, Cheng J, Liu Y, Li J and Jiang L 2012 High-temperature gating of solid-state nanopores with thermo-responsive macromolecular nanoactuators in ionic liquids *Adv. Mater.* **24** 962–7

[10] Yameen B, Ali M, Neumann R, Ensinger W, Knoll W and Azzaroni O 2009 Ionic transport through single solid-state nanopores controlled with thermally nanoactuated macromolecular gates *Small* **5** 1287–91

[11] Yameen B, Ali M, Neumann R, Ensinger W, Knoll W and Azzaroni O 2009 Synthetic proton-gated ion channels via single solid-state nanochannels modified with responsive polymer brushes *Nano Lett.* **9** 2788–93

[12] Tagliazucchi M, Azzaroni O and Szleifer I 2010 Responsive polymers end-tethered in solid-state nanochannels: when nanoconfinement really matters *J. Am. Chem. Soc.* **132** 12404–11

[13] Vlassiouk I, Park C-D, Vail S A, Gust D and Smirnov S 2006 Control of nanopore wetting by a photochromic spiropyran: a light-controlled valve and electrical switch *Nano Lett.* **6** 1013–7

[14] Wang G, Bohaty A K, Zharov I and White H S 2006 Photon gated transport at the glass nanopore electrode *J. Am. Chem. Soc.* **128** 13553–8

[15] Hoelz A, Debler E W and Blobel G 2011 *Annual Review of Biochemistry* vol 80, ed R D Kornberg *et al* pp 613–43

[16] Peleg O and Lim R Y H 2010 Converging on the function of intrinsically disordered nucleoporins in the nuclear pore complex *Biol. Chem.* **391** 719–30

[17] Fernandez-Martinez J and Rout M P 2012 A jumbo problem: mapping the structure and functions of the nuclear pore complex *Curr. Opin. Cell Biol.* **24** 92–9

[18] Alber F *et al* 2007 The molecular architecture of the nuclear pore complex *Nature* **450** 695–701

[19] Tagliazucchi M, Peleg O, Kröger M, Rabin Y and Szleifer I 2013 Effect of charge, hydrophobicity, and sequence of nucleoporins on the translocation of model particles through the nuclear pore complex *Proc. Natl Acad. Sci. USA* **110** 3363–8

[20] Patel S S, Belmont B J, Sante J M and Rexach M F 2007 Natively unfolded nucleoporins gate protein diffusion across the nuclear pore complex *Cell* **129** 83–96

[21] Ribbeck K and Görlich D 2002 The permeability barrier of nuclear pore complexes appears to operate via hydrophobic exclusion *EMBO J.* **21** 2664–71

[22] Colwell L J, Brenner M P and Ribbeck K 2010 Charge as a selection criterion for translocation through the nuclear pore complex *PLoS Comp. Biol.* **6** e1000747

[23] Ma J and Yang W 2010 Three-dimensional distribution of transient interactions in the nuclear pore complex obtained from single-molecule snapshots *Proc. Natl Acad. Sci.* **107** 7305–10

[24] Ma J, Goryaynov A, Sarma A and Yang W 2012 Self-regulated viscous channel in the nuclear pore complex *Proc. Natl Acad. Sci.* **109** 7326–31

[25] Peters R 2005 Translocation through the nuclear pore complex: selectivity and speed by reduction-of-dimensionality *Traffic* **6** 421–7

[26] Peleg O, Tagliazucchi M, Kroeger M, Rabin Y and Szleifer I 2011 Morphology control of hairy nanopores *ACS Nano* **5** 4737–47

[27] Tagliazucchi M, Olvera de la Cruz M and Szleifer I 2010 Self-organization of grafted polyelectrolyte layers via the coupling of chemical equilibrium and physical interactions *Proc. Natl Acad. Sci.* **107** 5300–5

[28] Huang K and Szleifer I 2017 Design of multifunctional nanogate in response to multiple external stimuli using amphiphilic diblock copolymer *J. Am. Chem. Soc.* **139** 6422–30

[29] Flory P J 1969 *Statistical Mechanics of Chain Molecules* (New York: Wiley)

[30] Weinan E, Ren W and Vanden-Eijnden E 2007 Simplified and improved string method for computing the minimum energy paths in barrier-crossing events *J. Chem. Phys.* **126** 164103

[31] Tagliazucchi M, Rabin Y and Szleifer I 2011 Ion transport and molecular organization are coupled in polyelectrolyte modified nanopores *J. Am. Chem. Soc.* **133** 17753–63

[32] Carignano M A and Szleifer I 1995 Structural and thermodynamic properties of end-grafted polymers on curved surfaces *J. Chem. Phys.* **102** 8662–9

[33] Grest G S and Murat M 1993 Structure of grafted polymeric brushes in solvents of varying quality: a molecular dynamics study *Macromolecules* **26** 3108–17

[34] Zwanzig R 1988 Diffusion in a rough potential *Proc. Natl Acad. Sci.* **85** 2029–30

[35] Putzel G G, Tagliazucchi M and Szleifer I 2014 Nonmonotonic diffusion of particles among larger attractive crowding spheres *Phys. Rev. Lett.* **113** 138302

[36] Coriell S R and Jackson J L 1963 Potential and effective diffusion constant in a polyelectrolyte solution *J. Chem. Phys.* **39** 2418–22

[37] Ting C L and Frischknecht A L 2013 Activated pathways for the directed insertion of patterned nanoparticles into polymer membranes *Soft Matter* **9** 9615–23

[38] Gleria I, Mocskos E and Tagliazucchi M 2017 Minimum free-energy paths for the self-organization of polymer brushes *Soft Matter* **13** 2362–70